3

Physical Problems Associated with Data Collection in CT

The main topic of this book is a discussion of the algorithms by which the distribution of the relative linear attenuation at an effective energy $\bar{e}$, namely $\mu_{\bar{e}}(x, y)$, is calculated from estimates of its line integrals along a finite number of lines. The measurements in CT are taken in order to estimate these line integrals. In this chapter we discuss the physical limitations and problems that arise in estimating the line integrals from the calibration and actual measurements. Except for the problems of photon statistics and beam hardening, our discussion will be limited to a summary of the problems with some indications on how their effects may be reduced. We also discuss the different scanner configurations that are used in computerized tomography. In Chapter 5 we illustrate the effects on the quality of the reconstruction of the different sources of error in the data collection.

3.1 Photon Statistics

A very basic limitation to the accuracy of measurements taken in CT is the statistical nature of the process of x-ray photon production, photon interaction with matter, and photon detection. We discuss these processes one by one.

Consider the experiment in which we count the actual number of photons emitted in a unit period of time in the direction of a detector by a stable x-ray source that emits on average λ photons in a unit period of time in the direction of the detector. Such an experiment gives rise to a discrete random variable, which we denote by Y_λ (see Section 1.2). The set S_{Y_λ} of the possible outcomes of the experiment consists of the nonnegative integers (the photon counts). In this book we accept without further discussion the physical result that

$$p_{Y_\lambda}(y) = \frac{\lambda^y \exp(-\lambda)}{y!}. \tag{3.1}$$

In Fig. 3.1 we show the values of $p_{Y_\lambda}(y)$ for $y = 0, \ldots, 50$ when (a) $\lambda = 5$ and (b) $\lambda = 25$.

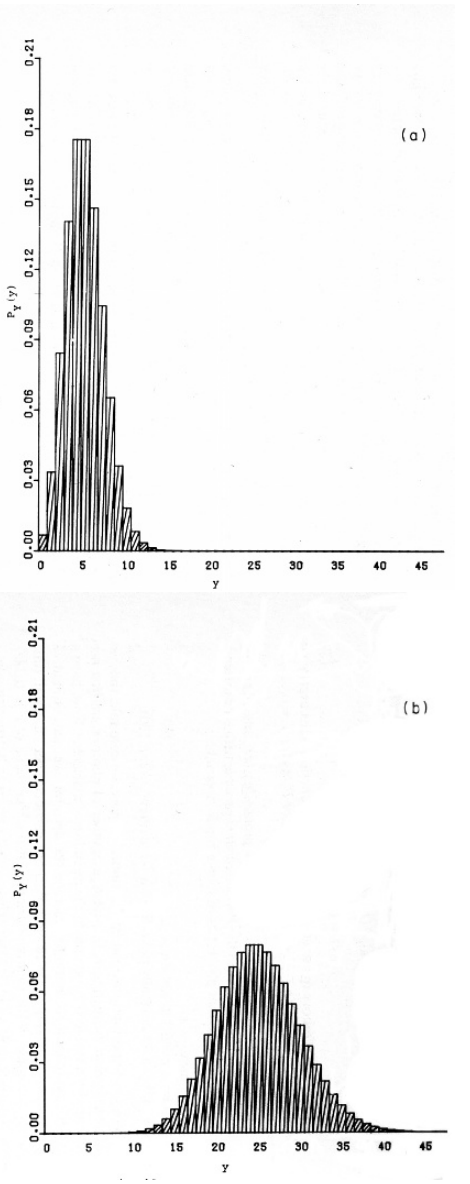

Fig. 3.1: Plots of the functions (a) p_{Y_5} and (b) $p_{Y_{25}}$ in (3.1).

Equation (3.1) is referred to as the *Poisson probability law*, and a discrete random variable Y_λ satisfying it is called the *Poisson random variable* with parameter λ. We note three important properties of this random variable:

(i) its mean is λ,

(ii) its variance is λ,
(iii) it is very similar to the Gaussian random variable X with mean λ and variance λ, as defined by (1.10), provided that λ is large (greater than 100), in the sense that, for any interval $(a, b]$ such that $b - a$ is a positive integer, $P_{Y_\lambda}(a, b] \simeq P_X(a, b]$.

This has important practical implications. Suppose, for example, that we are interested in estimating λ, the average number of photons emitted per unit time by a stable x-ray source in the direction of a detector. If we have a way of counting all the photons reaching the detector, we may estimate λ by the count of the number of photons during a particular period of unit time (i.e., by a sample of the random variable). If the true value of λ is 10,000, then there is at most a 1 in 20 chance that we make an error 200 (two standard deviations) or more using this approach. (Recall from Section 1.2 that we are 95% confident that the mean of a Gaussian random variable is within two standard deviations of a random sample from it.) Alternatively, we may count the number of photons for 100 units of time, and divide the count by 100 to give us an estimate of λ. The total number of photons during this longer period is on average 1,000,000, and in 19 cases out of 20, the actual count will be between 998,000 and 1,002,000. So in 19 cases out of 20, the estimate of λ will be between 9,980 and 10,020; i.e., the error is 20 or less. By increasing the time period used for counting photons by a factor of 100 we have reduced the size of the likely error in our estimate by a factor of 10. We observe a similar phenomenon in the following when we discuss how the accuracy of the calibration and actual measurements in CT is dependent on the total number of x-ray photons used.

Now we look at the statistical nature of the interactions of x-ray photons with matter. Suppose that a photon leaves the source in direction of the detector along a line L (see Fig. 2.4). Then there is a fixed probability ρ that the photon will get as far as the detector without being absorbed or scattered. This probability depends on the energy of the photon and the material intersected by the line L between the source and the detector. We call ρ the *transmittance* along L of the material between the source and the detector at that particular energy. If everything between the source and the detector remains stationary for a period of time and during this time 10,000 photons of the same energy leave the source in direction of the detector along the line L, then the number of photons reaching the detector will be approximately, but almost never exactly, $10{,}000\rho$. The rest of the photons will be absorbed or scattered.

A photon that reaches the detector is not necessarily counted. For each energy, there is a fixed probability that a photon that reaches the detector is counted by the detector. We call σ the *efficiency* of the detector at that particular energy. Continuing with the case discussed in the previous paragraph, the number of photons out of the original 10,000 that will not be absorbed

or scattered and will be counted is approximately, but almost never exactly, $10{,}000\rho\sigma$. The following important statement is proved in Section 15.5.

Let λ denote the average of the number of photons at energy $\bar{e}$ that are emitted in one unit of time by a stable x-ray source along a line L in the direction of a detector. Let ρ denote the transmittance along L of the material between the source and detector at energy $\bar{e}$. Let σ denote the efficiency of the detector at energy $\bar{e}$. Then the number of photons that

(i) are at energy $\bar{e}$,
(ii) reach the detector without having been absorbed or scattered, and
(iii) are counted by the detector in one unit of time,

is a sample of the Poisson random variable with parameter $\lambda\rho\sigma$.

We are now in position to discuss what is being measured during the data collection phase of CT, as described in Section 2.3. For this discussion we assume that the x-ray beam is monochromatic, the x-ray source and detectors are negligible in size (hence all photons from the source to the detector travel in the same straight line), and that a photon that has been absorbed or scattered along this line never reaches the detector. In subsequent sections we talk about the errors introduced by the physical unattainability of these assumptions.

Let us look at the exact nature of the process involved in getting the C_m and the A_m of (2.2). Suppose that a monochromatic x-ray source of energy $\bar{e}$ is such that the fraction of emitted photons that leave in the direction of the reference detector is ϕ_r, and the fraction of emitted photons that leave in the direction of the actual detector is ϕ_d (see Fig. 2.4). Suppose further that the averages of the total number of photons emitted during the periods of the calibration and actual measurements are λ_c and λ_a, respectively. Let ρ_r be the transmittance at energy $\bar{e}$ of the material between the source and the reference detector, and let ρ_c and ρ_a be the transmittance at energy $\bar{e}$ of the material between the source and the actual detector during the calibration and the actual measurement, respectively. Let σ_r, respectively σ_d, be the efficiency at energy $\bar{e}$ of the reference detector, respectively of the detector.

Consider now how we get a value of C_m. The actual number of photons emitted is a sample y_c from Y_{λ_c}. The actual number of photons counted by the reference detector is a sample c_r from the binomial distribution with parameters y_c and $\phi_r\rho_r\sigma_r$ and the actual number of photons counted by the actual detector is a sample c_a from the binomial distribution with parameters y_c and $\phi_d\rho_c\sigma_d$. To avoid divisions by zero and (later on) having to take the logarithm of zero, in the unlikely case that either c_r or c_a is 0, we set its value to 1. Finally, we define $C_m = c_a/c_r$. This is quite a complicated sampling process, especially since c_r and c_a are related to each other by the fact that the binomial distributions from which they are picked have the parameter y_c in common, but this parameter itself changes from sample to sample.

Ignoring the full complexity of the statistics for the moment, let us argue based just on means. The means of the binomial distributions with parameters

y_c and $\phi_r\rho_r\sigma_r$ and with parameters y_c and $\phi_d\rho_c\sigma_d$ are $y_c\phi_r\rho_r\sigma_r$ and $y_c\phi_d\rho_c\sigma_d$, respectively. Hence, it is reasonable to claim that

$$C_m \simeq \phi_d\rho_c\sigma_d/\phi_r\rho_r\sigma_r. \tag{3.2}$$

By a completely analogous argument for the actual measurement process, we obtain that

$$A_m \simeq \phi_d\rho_a\sigma_d/\phi_r\rho_r\sigma_r. \tag{3.3}$$

Combining (3.2) and (3.3) with (2.2), we get that

$$m \simeq -\ln(\rho_a/\rho_c). \tag{3.4}$$

In Section 15.2 we show that

$$-\ln\frac{\rho_a}{\rho_c} = \int_0^D \mu_{\bar{e}}(x,y)\,dz. \tag{3.5}$$

This is why the monochromatic ray sum m can be used as an estimator to $\int_0^D \mu_{\bar{e}}(x,y)\,dz$ in an algorithm that calculates $\mu_{\bar{e}}(x,y)$ at individual points from the line integrals of $\mu_{\bar{e}}(x,y)$ (see Section 2.6).

The important question is: How accurate an estimator is m of $-\ln(\rho_a/\rho_c)$? As illustrated in Section 15.5, in a realistic CT situation, it can be assumed that m is a sample of a random variable M such that

$$|\mu_M + \ln(\rho_a/\rho_c)| < S, \tag{3.6}$$

and

$$V_M \simeq S, \tag{3.7}$$

where

$$S = (\phi_d\lambda_a\rho_a\sigma_d)^{-1} + (\phi_r\lambda_a\rho_r\sigma_r)^{-1} + (\phi_d\lambda_c\rho_c\sigma_d)^{-1} + (\phi_r\lambda_c\rho_r\sigma_r)^{-1}. \tag{3.8}$$

If we can make this quantity S very small, then we ensure accurate estimation of $-\ln(\rho_a/\rho_c)$ by m.

Note that one way of making S very small is to make the number of photons leaving the source (λ_c and λ_a) large. Except for the problem of possibly saturating the counting capability of the detectors there is no difficulty in making λ_c very large, and thereby making the last two terms in S negligibly small. In such a case we see that S becomes inversely proportional to λ_a. Unfortunately, one cannot make the number of photons leaving the source during the actual measurement arbitrarily large, since this would result in an unacceptable radiation dose to the patient and may slow the process of projection taking so that errors due to motion become important (see the following). Note, however, that by ensuring that ϕ_r is much larger than ϕ_d and that the transmittance ρ_r between the source and the reference detector is relatively large (near 1), it is possible that we can also make the second term (3.8) negligibly small. This leaves us with

$$S \simeq 1/\phi_d \lambda_a \rho_a \sigma_d, \tag{3.9}$$

which shows in particular that the error in our estimation of $-\ln(\rho_a/\rho_c)$ depends on the transmittance ρ_a during the actual measurement; lesser transmittance results in greater error.

As can be seen from the preceding, a certain amount of error in the measurements due to the statistical nature of the processes of x-ray photon production, photon interaction with matter, and photon detection is unavoidable. The properties of the error, considered as a random variable, are understood. As we shall see, some reconstruction algorithms attempt to make use of these properties. Since the errors in the measurements affect the outcome of the reconstruction process, it is important to understand both the nature of these errors and the way in which the results produced by a given reconstruction algorithm are influenced by such errors.

3.2 Beam Hardening

The x-ray beam used in CT is polychromatic, consisting of photons at different energies. Because the attenuation at a fixed point is generally greater for photons of lower energy, the energy distribution spectrum of the x-ray beam changes (hardens) as it passes through the object. X-ray beams reaching a particular point inside the body from different directions are likely to have different spectra (having passed through different materials before reaching the point in question) and thus will be attenuated differently at that point. This makes it difficult to assign a single value to the attenuation coefficient at a point in the body.

A possible solution to this difficulty is to assign to the point the attenuation coefficient of photons at a particular energy (what we referred to as the effective energy). If we used monochromatic x-ray beams consisting of photons only at that single energy, beams from different directions would be attenuated in the same way at a fixed point. Reconstruction of such attenuation coefficients is a well-defined aim of computed tomography.

In this section we discuss mathematical formulas that describe the nature of polychromatic ray sums and methods that may be used to find the corresponding monochromatic ray sums. It is shown in Section 15.6 that the polychromatic ray sum p approximates an integral of the form

$$p \simeq -\ln \int_0^E \tau_e \exp\left(-\int_0^D (\mu_e(z) - \mu_e^a)\, dz\right) de. \tag{3.10}$$

We now give a detailed explanation of the meaning of the symbols in (3.10).

It is assumed that the source emits a polychromatic x-ray beam with photons at energies between 0 and E. We use τ_e to denote the value at energy e of the probability density function of the continuous random variable that

describes the statistical distribution of the energies of the photons counted during the calibration measurement. Here we have adopted the somewhat nonstandard notation of using τ_e to denote the value of a function of energy at the energy e. We refer to this probability density function as the *detected spectrum during the calibration measurement*.

The symbols D and z have the same meaning as in the last chapter (see Fig. 2.4) and $\mu_e(z)$ is a function of two variables (the energy e and the distance z), whose value is the linear attenuation coefficient at energy e at the point z on the line L during the actual measurement. On the other hand, μ_e^a is a function of one variable only (the energy e), whose value is the linear attenuation of the reference material a at energy e. Thus, $\int_0^D (\mu_e(z) - \mu_e^a)\, dz$ is the integral of the relative linear attenuation at energy e along the line L. Note, in particular, that the polychromatic ray sum depends only on the relative linear attenuations (at all energies between 0 and E) and on the detected spectrum during the calibration measurement. Rewriting (2.4) in this notation we get

$$m \simeq \int_0^D (\mu_{\bar{e}}(z) - \mu_{\bar{e}}^a)\, dz. \tag{3.11}$$

Recall now that CT numbers represent relative linear attenuations at the effective energy $\bar{e}$; and that they are to be obtained from estimates of the monochromatic projection data, which are themselves calculated from the experimentally obtained polychromatic projection data. The method of estimating the monochromatic projection data from the polychromatic projection data is the topic of the rest of this section.

We start with a theoretical discussion of a special situation. Suppose that during the actual measurement there are only two types of material, a and b, in the reconstruction region (a is the reference material). Consider a fixed source–detector pair, and assume that the total length of the parts of the line L that go through material b is B. From (3.10) and (3.11) we get

$$p \simeq -\ln \int_0^E \tau_e \exp\left(-B\left(\mu_e^b - \mu_e^a\right)\right) de \tag{3.12}$$

and

$$m \simeq B\left(\mu_{\bar{e}}^b - \mu_{\bar{e}}^a\right). \tag{3.13}$$

Combining (3.12) and (3.13) we get

$$p \simeq -\ln \int_0^E \tau_e \exp\left(-\frac{\mu_e^b - \mu_e^a}{\mu_{\bar{e}}^b - \mu_{\bar{e}}^a} m\right) de. \tag{3.14}$$

The important thing to observe in (3.14) is that, provided either $\mu_e^b > \mu_e^a$ for all energies between 0 and E or $\mu_e^b < \mu_e^a$ for all energies between 0 and E, its right-hand side is a monotonic function of m. (Note that τ_e is positive for all e.) Hence, given any value of p, there is only one value of m that makes

the two sides of (3.14) equal. In practice we can use the plot of the right-hand side of (3.14) to correct for beam hardening; we simply find the value of m for which the value of the right-hand side is the experimentally obtained polychromatic ray sum p.

Equation (3.14) was obtained under the rather restrictive assumption that there are only two different types of material in the reconstruction region. If the organ we are looking at is a head inserted into a water bag, this assumption is not too badly violated, since the contents of the head are bone and material whose x-ray attenuation properties are not too dissimilar to water. Thus (3.14) may be used for correcting for beam hardening in such a situation, but in general it is not as good as some other methods to be discussed in the following.

While the precise method based on (3.14) must be considered to be unreliable because of the too restrictive nature of the underlying assumptions, the general approach suggested by it is very attractive: specify a function q of the polychromatic ray sum p such that if we use $q(p)$ as our estimate of the monochromatic ray sum m, then we get reasonably good reconstructions of the relative linear attenuations at the effective energy $\bar{e}$.

Natural candidates for such a function are *polynomials*, i.e., functions of the form

$$q(p) = a_n p^n + a_{n-1} p^{n-1} + \cdots + a_1 p + a_0, \tag{3.15}$$

where n (the order of the polynomial) is a fixed integer and $a_0, \ldots, a_n$ are fixed coefficients that need to be determined so that $q(p)$ provides an acceptable estimate of m for our purpose. There are two computational advantages of polynomial approximations to others (for example, approximation by combination of exponentials): the coefficients are easy to calculate and, once they are calculated, (3.15) is easy to evaluate, especially since a low value of n (less than 5) usually suffices (see Section 5.6).

In certain cases there is no single function q such that replacement of m by $q(p)$ in (2.5) would lead to acceptable reconstructions. One is then forced to use either multiple correcting functions specific to the source–detector pair positions or an iterative correction procedure, where the correcting function q for the next iteration is based on a reconstruction during the previous iteration (see Section 5.6).

3.3 Other Sources of Error

If we wish to base our reconstruction algorithm on (2.5), then we have to know the values of $m(l, \theta)$ (the line integral of $\mu_{\bar{e}}(x, y)$ along L, see Fig. 2.4) for certain l and θ (i.e., for certain lines L). Photon statistics and beam hardening are two reasons why physical measurements can provide us only with approximations of $m(l, \theta)$. In this section we briefly discuss further reasons.

One source of error is that both the x-ray source (more precisely the focal spot of the x-ray source) and the detector have a certain size, and thus the

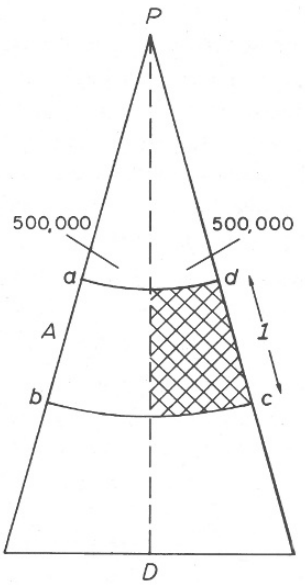

Fig. 3.2: Illustration of the partial volume effect.

photons that are counted do not all travel along the same line, but rather they travel along one of a bundle of lines forming a rather complicated shape.

One consequence of the non-negligible size of the focal spot and detector is the so-called *partial volume effect*, which we now explain on a simple two-dimensional example. Suppose we have a point monochromatic x-ray source P and a line segment detector D; see Fig. 3.2. Suppose that the linear attenuation coefficient (see Section 2.4) is everywhere zero except in that half of the area A that is cross-hatched in Fig. 3.2, where its value is two. It is assumed that the length of intersection with A of any line from P to D is unity. Suppose also that the reference material has linear attenuation coefficient zero (vacuum) and that the number of photons read by the reference detector during both calibration and actual measurement is 1000. Hence the number of photons that leave the source in direction of the detector is about the same during calibration and actual measurement. Suppose this number is 1,000,000. Thus the calibration measurement is $C_m \simeq 1000$. Breaking the x-ray beam into two equal halves as shown in Fig. 3.2 we see that approximately 500,000 photons will enter both halves of A. In the left half, where the linear attenuation coefficient is zero and hence transmittance is one, all 500,000 photons reach the detector. In the right half, where the linear attenuation is two, and hence transmittance is $e^{-2} \simeq 0.135$, the number of photons that reach the detector is about 68,000. Hence the total number of detected

photons is about 568,000 and the actual measurement is $A_m \simeq 568$. Using (2.2) we get $m \simeq 0.566$. This is an estimate, see (2.4), of the average of the line integral of the relative linear attenuation between the source and points on the detector. However, it is easy to see that the true value of this average is 1.0. The reason for this rather large error (43.4%) in the estimation of the average is that the beam is only partially blocked by attenuating material and the processes of taking exponentials and logarithms give a disproportionately great importance to the unblocked portion of the beam.

In principle, one can reduce the size of the source and the detector by putting lead shielding with long narrow pinholes in front of both of them, but this would have two undesirable consequences. One is that the error due to photon statistics would considerably increase, because the value of ϕ_d in (3.9) would become very small. The second consequence arises when we search for possibly small features in large organs (such as tumors in the lung) by taking cross-sectional slices. If the physical slices are thin, we have to use many slices to ensure that we do not miss what we are looking for. This results in longer time to be spent by the computer that provides the reconstructions and possibly by the radiologist who needs to examine them.

We have just given one example of a phenomenon that is rather common in CT: methods that can be used to combat error due to one physical phenomenon result in increasing the error due to another one. A further example of this is the way one handles *motion artifacts*.

It is an underlying assumption in CT that the $m(l, \theta)$, which we try to measure, are integrals along different lines of the same function $\mu_{\bar{e}}(x, y)$. However, this assumption is violated if some of these lines L go through a moving organ, such as the lung or the heart, and if the actual measurements are taken at different times for different lines, since the function $\mu_{\bar{e}}(x, y)$ changes as the organ moves. One way of combating this is to use multiple arrays of detectors and possibly even multiple sources (more about this in the next section), so that all the measurements can be taken within a small period of time during which organ motion is insignificant. However, this results in an increase of error due to detection of *scattered* photons, a phenomenon that we now discuss.

Note that in Section 3.1 we have assumed that the detector counts a photon only if it has left the source in the direction of the detector and has reached the detector without having been absorbed or scattered. If there is a single source and a single detector, this is a reasonable assumption, since a scattered photon can reach the detector only if it has been scattered in a direction very nearly the same as its original direction or if it has been multiply scattered away from and then back towards the detector. These events are sufficiently unlikely, so that the error due to scatter in a single source single detector case is rather small. However, if we have an array of detectors, a photon scattered out of its path towards one detector may very well reach another detector and be counted by it. Since the ratio of scattered photons to unscattered photons that reach a detector is dependent on the object to be reconstructed (and in a rather complicated way), the error introduced by scatter cannot be completely

removed from the measurements prior to reconstruction. Collimation, which absorbs photons coming towards a detector from directions other than the source, can reduce the number of scattered photons that are counted by the detector.

Finally, we discuss some errors that are due to the device used for collecting the data not functioning exactly as intended.

It is important that the source and the detectors do not change their behavior between the calibration measurement and the actual measurement. For example, in our derivation in Section 3.1 we have assumed that the efficiency σ_d, of the detector is the same during the calibration and the actual measurement. Change in detector efficiency would make (3.4) invalid.

Detector efficiency is assumed to be independent of the number of photons the detector has to count. This may be difficult to achieve in practice, since detectors can be saturated by too many photons getting to them. One way of combating this is by insertion of a compensator (see Fig. 2.4) that ensures that even along lines that either miss or hardly touch the object to be reconstructed, the total attenuation is significant enough for the detector not to get saturated. Alternatively, one can achieve this by using water as the reference material into which one inserts the object to be reconstructed during the actual measurement. One reason for preferring the former of these two methods is that it requires less radiation dose to achieve the same photon statistics. (This is because in the latter option photons that have already transited through the patient's body may get absorbed and so not reach the detector.)

Mechanical stability is also of importance; the lines along which data are collected should be the same lines that the algorithms assume as the lines of data collection.

There are other possible sources of errors in data collection, but their discussion is beyond the scope of this book.

3.4 Scanning Modes

Figure 3.3 shows five classical designs that had been used by devices for data collection in CT. While various variants of these scanning modes existed, we restrict our attention to these five basic modes. We discuss some of the advantages and disadvantages of each from the point of view of their proneness to the errors we have discussed in the previous section. This will be followed by a discussion of the scanning mode that is considered state-of-the-art for commercial scanners at the time of writing this revised edition.

In the first scanning mode, see Fig. 3.3(a), there is a single x-ray source and a single detector. There are two motions involved. First, both the detector and the source are moved in parallel in a direction perpendicular to the line connecting the source to the detector. During this time projection data are collected for one set of parallel lines. Second, the apparatus is rotated by a

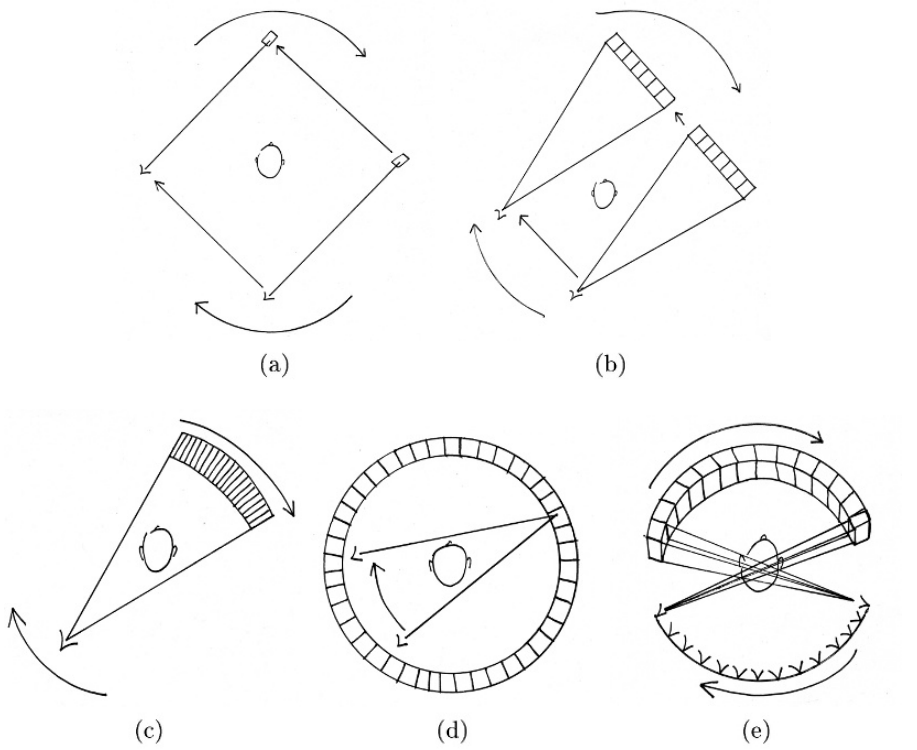

Fig. 3.3: Classical scanning modes in CT. (a) Pencil beam "incremental" scanner (single source, single detector, translate-rotate). (b) Fan beam "incremental" scanner (single source, multiple detector, translate-rotate). (c) Fan beam "spinning" scanner (single source, multiple detector, rotate only). (d) Fan beam "spinning" scanner (single rotating source, stationary ring of detectors). (e) Cone beam "cylindrical" scanner (multiple source, multiple-planar detector).

small amount (e.g., 1°). By repetition of these two motions, data are collected for a number (e.g., 180) of sets of parallel lines.

There are a number of attractive features of this method of data collection. There is very little noise due to scatter. The detector can be calibrated at the beginning of each of the parallel scans, since we can ensure that the first line of a scan misses the reconstruction region. The source–detector combination can be moved in small steps, ensuring that enough data are collected for reconstruction. (There will be more about this in later chapters.) An undesirable feature of this method of data collection is the time it takes; typically several minutes. Such a scanning mode is inappropriate for imaging organs that cannot stay stationary for more than a few seconds, such as the lung.

The second scanning mode in Fig. 3.3(b) was introduced to speed up the data collection process without losing most of the desirable features of the first scanning mode. Instead of one detector, an array of detectors is used (e.g., 30). As the source and detector array move in parallel, data are collected for several sets of parallel lines. When the apparatus is rotated, the rotation can be by a much larger angle than in the first scanning mode (e.g., 10^o), and yet the total number of sets of parallel lines is usually increased. Such scanners can collect all their data in slightly over 10 seconds, an acceptable breath holding period for most patients. Apart from increase in cost, the only obvious disadvantage of this scanning mode over the first one is the increased effect of scatter.

The third scanning mode in Fig. 3.3(c) involves only one motion. A single x-ray source is faced by a large enough array of detectors so that the angle subtended by the detector array at the source encloses the whole reconstruction region. The source and detector-array combination rotates around the patient. The data are collected for a large number of sets of lines (typically of the order of 500 sets with about the same number of lines in each); the lines in each set diverge from the source position to the detectors in the array. All data for one set are collected simultaneously. The complete data collection can be achieved in a matter of seconds (typically five or less). One potential problem with this arrangement is that calibration has to be done before the patient is inserted for possibly a whole series of scans, since in all positions of the apparatus the line between the source and the central detectors goes through the patient. Very stable detectors seem to have overcome this difficulty. Also, the detectors have to be narrow so that sufficient amount of data are collected for the reconstruction. This method of data collection was standard for commercial CT scanners for about twenty years from the late 1970s.

An alternative fast method of data collection, with only one motion, is the fourth scanning mode in Fig. 3.3(d). A stationary array of detectors has the x-ray source move inside it in a circle. The line from one of the detectors to the source forms a diverging set of lines as the source moves. Calibration of the detector for this set of lines is possible while the line from the detector to the source is outside the reconstruction region. The number of detectors has to be large compared with the previous scanning mode, unless one is willing to have radiation that goes through the body but ends up between detectors. The latter is undesirable, since the body is subjected to potentially harmful radiation that does not contribute diagnostic information. Also, it is more difficult to reduce scatter by collimation than in the previous scanning mode since the direction from detector to source changes as the source moves.

None of these scanning modes is appropriate for precise imaging of a rapidly moving organ such as the heart. Not only is the speed of data collection far too slow (the heart goes through a whole cycle in about one second), but also it is difficult to achieve a slice-to-slice coherence if the data are collected at different times for each cross-sectional slice. The fifth scanning

mode, Fig. 3.3(e), was designed to overcome these difficulties. An array of x-ray sources (e.g., 28) is arranged in a semicircle. They can be electronically switched on and off. They project the body onto a curved fluorescent screen, so that when an x-ray source is switched on a large part of the body (say the whole thorax) is imaged simultaneously, providing us with projection data for a cone beam of lines diverging from the source. It is possible to complete the data collection in as little as one-hundredth of a second, removing any possibility of organ motion interfering with the reconstruction process. Note that this method of data collection is essentially different from the other four, inasmuch as a series of two-dimensional projections of a three-dimensional object is collected rather than a series of one-dimensional projections of a two-dimensional object. While this arrangement solves the problems that motivated its introduction, it has its own special difficulties. For example, the number of views that can be taken is severely limited both by the cost and the size of the x-ray tubes, and the error due to scatter is unavoidably much more significant than in the previous scanning modes. It is also very expensive, especially if the whole sources–detectors combination needs to be rotated around the patient for high spatial resolution in the reconstructions. For such reasons, this scanning mode has not made it into clinical practice.

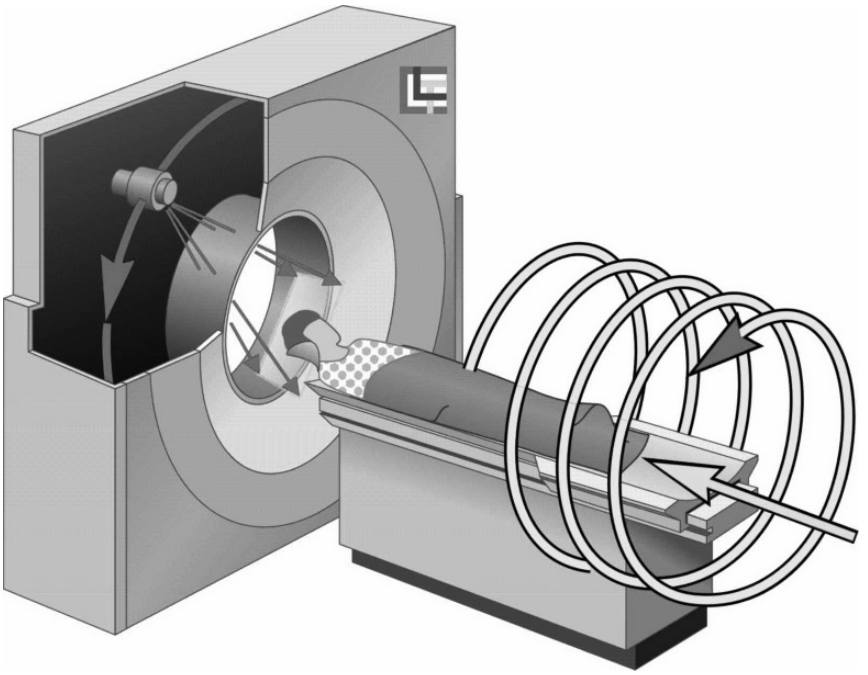

Fig. 3.4: Helical (also known as spiral) CT. (Illustration provided by G. Wang of the Virginia Polytechnic Institute & State University.)

Helical CT (also referred to as *spiral CT*) first started around 1990 and has become standard for medical diagnostic x-ray CT. Typically such a system is single source and multiple detectors (which were initially in a single one-dimensional array as in Fig. 3.3(c), but then were replaced by detectors in a two-dimensional array similar to the detectors in Fig. 3.3(e)); the innovation over the previously mentioned scanning modes is the presence of an independent motion: while the source–detectors rotate around the patient, the table on which the patient lies is continuously moved between them (typically orthogonally to the plane of rotation), see Fig. 3.4. Thus, the trajectory of the source relative to the patient is a helix (hence the name "helical CT"). Helical CT (especially in its cone-beam mode) allows rapid imaging as compared with the previous commercially-viable approaches, which has potentially many advantages. One example is when we wish to image a long blood vessel that is made visible to x-rays by the injection of some contrast material: helical CT may very well allow us to image the whole vessel before the contrast from a single injection washes out and this may not be possible by the slower scanning modes. Since our mathematical and algorithmic development in this book is mainly devoted to the reconstruction of two-dimensional slices from one-dimensional projections (as in Figs. 2.4 and 3.3(c)), we do not get into further discussion of helical CT here. We return to the topic in Chapter 13, where we illustrate the data collection for a dynamically changing object using helical CT and an algorithm for reconstructing the object from such data. We point out that the CT scanners illustrated in Fig. 1.4 are in fact modern helical CT scanners, but at the level of detail of that figure they could just as well be used as illustrations for the older fan beam spinning scanners whose nature is indicated in Fig. 3.3(c).

There are many existing and possible variants of these scanning modes, and many more advantages and disadvantages to each than we have space to mention. However, the configurations discussed here include all the basic arrangements that we need to consider when discussing reconstruction algorithms.

Notes and References

Justification for using the Poisson probability law to describe photon generation can be found in standard books, such as [77]. More detailed discussion of the nature of Poisson random variables is also a standard topic; see, e.g., [217]. A recent paper discussing the noise properties of sinograms in x-ray CT is [267].

The material on beam hardening is based on [111], which gives many early references. An example of an iterative beam-hardening correction procedure is given in [153]. A comparative study is reported in [141]. Examples of recent developments on beam-hardening correction (from the nondestructive testing literature) are [163, 264]. We return to this topic in Section 5.6. It was

pointed out in [192] that general-purpose beam-hardening correction methods may, under some circumstances, result in a so-called pseudo-enhancement, which may result in an incorrect diagnosis. This clinically important issue was subsequently addressed in a number of papers; a recent example is [209]. An alternative to correcting for beam hardening is to attempt to make use of the nature of the x-ray spectrum. An early example of such an approach was proposed in [7, 191]. For a much more recent approach see [222].

The shape of the x-ray beam in CT, and what one might do about the errors introduced by it, is discussed in [26]. A discussion of the partial volume is given in [95]. The nature of scatter and correction for it is dealt with in [252]; see also [78].

The first commercially available CT scanner was manufactured by EMI Ltd; see [146]. This scanner was of the type shown in Fig. 3.3(a). A scanner of the type shown in Fig. 3.3(c) is reported on in [70]; see also [218]. A scanner of the type shown in Fig. 3.3(e) is the dynamic spatial reconstructor (DSR) reported on in [232] and its use for imaging physiological functions was detailed in [231]. A table of the physical characteristics of the early commercial scanners is given by [32]. Our classification of classical scanning modes is based on that provided in [271].

A recent article on helical (spiral) CT is [266], it gives a good survey of this very important development. A book that also deals with this topic is [155]. Two early papers are [58, 156]. Sample papers that report on recent technological and application developments of helical CT are [279] and [87], respectively.

In this chapter, as indeed in the whole of this book, we have concentrated on x-ray CT. Data collection in other applications of image reconstruction from projections will have their own physical problems; for a recent example see [22] that discuses a model of noise in low-dose electron microscopy.